Growth and spectroscopic characteristics of Nd-doped $PbWO_4$ crystal*

Wang Qing-Guo(王庆国)[a)b)], Su Liang-Bi(苏良碧)[a)], Li Hong-Jun(李红军)[a)], Xiong Wei(熊 巍)[a)], Yuan Hui(袁 晖)[a)], Zheng Li-He(郑丽和)[a)], Xu Xiao-Dong(徐晓东)[a)], Wu Feng(吴 锋)[a)], Tang Hui-Li(唐慧丽)[a)], Jiang Da-Peng(姜大朋)[a)], and Xu Jun(徐 军)[a)†]

[a)] *Key Laboratory of Transparent and Opto-Functional Inorganic Materials, Shanghai Institute of Ceramics, Chinese Academy of Sciences, Shanghai* 201800, *China*

[b)] *Graduate University of the Chinese Academy of Sciences, Beijing* 100039, *China*

(Received 22 September 2011; revised manuscript received 2 November 2011)

Nd-doped $PbWO_4$ crystals are grown by using the modified Bridgman method. The spectroscopic properties of the crystals are investigated. The changes of the absorption band at 350 nm are discussed for samples annealed at 740 °C and 1040 °C. The radiative lifetime of the $^4F_{3/2}$ level is calculated by using the Judd–Ofelt theory according to the absorption spectrum of 0.5 at.% Nd-doped $PbWO_4$ crystal. The spontaneous Raman scattering properties of the crystals are analysed.

Keywords: $PbWO_4$, Bridgman method, Judd–Ofelt theory, Raman spectra

PACS: 42.70.Hj, 42.62.Fi, 61.72.Cc, 81.10.Fq **DOI:** 10.1088/1674-1056/21/5/054217

1. Introduction

In recent years, rare-earth-doped laser materials and their spectroscopic properties have been widely investigated. New laser crystals and new laser output wavelengths are the focus of this field.[1−7] In particular, stimulated Raman scattering (SRS) has become a well-established technique for shifting the frequency of the laser radiation to new spectral regions where direct laser oscillation is not available or ineffective. Raman active media doped with laser active ions form self-stimulated Raman laser crystals. Acting as both the laser crystal and the Raman medium, self-stimulated Raman laser crystals are useful for simplifying laser optical systems and realizing the miniaturization and integration of lasers. In 1999, the self-stimulated Raman scattering laser output of Nd-doped $KGd(WO_4)_2$ crystal was achieved under semiconductor laser pumping, and its largest Stokes laser output power reached up to 4.8 mW.[8]

Lead tungstate crystal ($PbWO_4$), known as the scintillator and the stimulated Raman-scattering-active medium, has been widely investigated since its luminescence was reported in 1948.[9,10] The structural defects and the optical properties of the as-grown and the annealed $PbWO_4$ crystals were investigated.[11−14] Rare-earth-doped $PbWO_4$ crystals have been used as solid-state laser media, especially as self-stimulated Raman laser crystals.[15−18]

In 2000, Kaminskii *et al.*[11] carried out detailed investigations of the Raman spectra and the Raman lasers of $PbWO_4$ crystals. A total Stokes conversion efficiency beyond 50% has been achieved. Pulsed and the continuous-wave laser actions in Nd^{3+}-doped $PbWO_4$ crystal have also been realized.[11,15] Chen *et al.*[16] obtained a self-stimulated Raman laser of Nd^{3+}-doped $PbWO_4$ crystal with 56% optical frequency conversion efficiency in 2001.

In this work, we grow Nd-doped $PbWO_4$ crystals with different Nd concentrations by using the modified Bridgman method. The spectroscopic properties of the as-grown and the annealed samples are investigated. Then, the Raman spectra of the crystals are recorded, and their stimulated Raman properties are discussed.

2. Crystal growth

The Nd-doped $PbWO_4$ crystals were grown by using the modified Bridgman method.[19] The $PbWO_4$

*Project supported by the National Natural Science Foundation of China (Grant Nos. 60938001, 60908030, 61178056 and 51002175) and the Hundred Talent Project of the Chinese Academy of Sciences.

†Corresponding author. E-mail: xujun@mail.shcnc.ac.cn

© 2012 Chinese Physical Society and IOP Publishing Ltd

polycrystalline scraps obtained from the crystallization process were used as the raw material for growing the crystals. Pt crucibles were used in this work. Three crystals with different concentrations of Nd^{3+} ions were grown, i.e., 0.2 at.%, 0.5 at.%, and 1.0 at.% (denoted as A, B, and C, respectively). The crystals were grown at 1130 °C. The ⟨001⟩-cut $PbWO_4$ crystals were used as the seeds. The decline rate of the crucible was 1.0 mm/h. A photo of crystal C is shown in Fig. 1. The cross-section of the crystal is about 3.0 cm×3.0 cm.

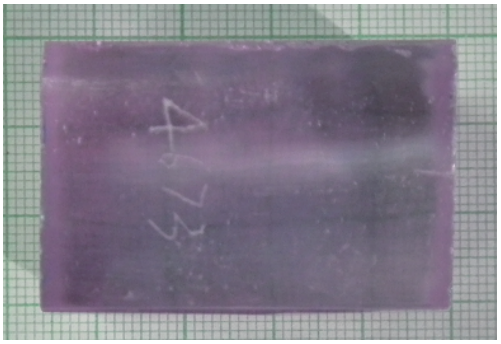


Fig. 1. (colour online) Photo of the 1.0 at.% Nd-doped $PbWO_4$ crystal.

The samples used for the measurements were c-plane wafers with a thickness of 3 mm. Absorption spectra were recorded using a Lambda 1050 UV–visible–near-infrared (UV–VIS–NIR) absorption spectrophotometer. The luminescence spectrum at 830–1500 nm was measured with a Triax550 spectrofluorimeter under 808 nm laser diode (LD) pumping. The emission lifetime of the $^4F_{3/2}$ level was measured using a modulated 808 nm laser diode with a Tektronix TDS3052 digital oscilloscope for recording the temporal decay curves of the fluorescence signals at around 1060 nm. The backscattered Raman spectra excited by a 514 nm laser were recorded using an Invia Raman Microscope (Renishaw, England). All measurements were taken at room temperature.

3. Results and discussion

3.1. ICP-AES analysis

The concentrations of the impurities at different locations in the crystals were measured by inductively coupled plasma atomic emission spectroscopy (ICP-AES) analysis (Table 1). The samples were selected from the top (away from the seed, C_T) and the bottom (near the seed, C_B) parts of the crystals. The segregation coefficients of the dopant ions were calculated with the formula $k = C_S/C_L$, which is the ratio of the concentration of solute in the solid (C_S) to that in the liquid (C_L). At the beginning of the crystal growth, C_S was the solute concentration near the seed, and C_L could be approximately replaced by the original concentration of the solute (C_0). So, the segregation coefficients of the Nd^{3+} ions in the three crystals were 1.0, 0.83, and 0.62, respectively.

Table 1. Concentrations of Nd^{3+} ions in different parts of the grown crystals.

Crystal	C_T/wt.%	C_B/wt.%	C_0/wt.%	k
A	0.028	0.074	0.074	1.0
B	0.10	0.15	0.18	0.83
C	0.21	0.23	0.37	0.62

3.2. Room temperature absorption properties

The absorption spectra of the as-grown crystals are shown in Fig. 2. Their absorption cross-sections can be obtained using the equation $\sigma_{abs} = O_D(\lambda)/0.433dN$, where $O_D(\lambda)$ is the absorption optical density of the crystal at wavelength λ, $O_D(\lambda) = \lg(I_0/I)$ with I_0 and I being the intensities of the incident and the transmitted light, respectively, d is the thickness of the sample, and N is the concentration of the dopant ions in the sample. The cross-sections obtained are 2.85×10^{-20} cm^2, 3.11×10^{-20} cm^2, and 2.88×10^{-20} cm^2, respectively. The absorption cross-section of Nd^{3+}-doped $PbWO_4$ crystal is smaller than those of Nd^{3+}-doped vanadate and tungstate crystals, such as Nd^{3+}-YVO_4 (57×10^{-20} cm^2), Nd^{3+}-$GdVO_4$ (52×10^{-20} cm^2), Nd^{3+}-$LuVO_4$ (69×10^{-20} cm^2), Nd^{3+}-KYW (4.56×10^{-20} cm^2), and Nd^{3+}-KGW (3.82×10^{-20} cm^2).[20–26]

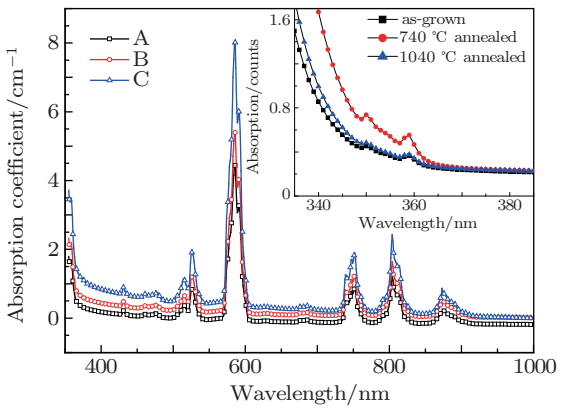


Fig. 2. (colour online) The absorption spectra of the Nd-doped $PbWO_4$ crystals. The inset shows the absorption spectra around 350 nm of the as-grown and the annealed crystal B.

The reported experimental results have shown that the annealing treatment in air can effectively modulate the microstructure of as-grown $PbWO_4$ crystal through reducing the intrinsic defects and then improve its radiation intensity and optical performances.[10,27,28] The absorption spectra around 350 nm for sample B annealed at 740 °C and 1040 °C for 8 h respectively are shown in the inset of Fig. 2. Compared with that of the as-grown crystal, as the annealing temperature increases from 740 °C to 1040 °C the absorption intensity of crystal B first increases and then decreases. It is well known that the absorption around 350 nm originates from the associated defect $[V_F^-–V_o–V_F^-]$, where V_F^- is an O_2^{3-} hole trapped by a lead vacancy, and V_o is an oxygen vacancy.[29] So, the concentration of $[V_F^-–V_o–V_F^-]$ increases under the 740 °C annealing process and decreases as the temperature increases from 740 °C to 1040 °C. When the $PbWO_4$ crystal is heated in air, the oxygen from the air will diffuse into the lattice to fill the oxygen vacancies, which will induce two holes (h) in the crystal, i.e., $PWO + V_o + 1/2O_2 \rightarrow O_o^x + 2\,h$. And at the same time, O^{2-} ions at regular positions (O_o^x) will obtain enough energy to jump over the potential barrier around the atom to form an interstitial oxygen (O_i) and an oxygen vacancy, i.e., $PWO + O_o^x \rightarrow O_i + V_o$ (the Frenkel defect reaction). When the crystal is annealed under 740 °C, the first process will be dominant due to the larger formation energy needed for the latter one. In the annealing process, the increase of holes will induce the formation of $[V_F^-–V_o–V_F^-]$ clusters, i.e., $2\,h + 2V_c^* + V_o \rightarrow [V_F^-–V_o–V_F^-]$, which can increase the absorption at 350 nm.

With the annealing temperature increasing, a Frenkel defect reaction will occur in the crystal. So, the concentration of V_o will increase. The positive mobile V_o may decompose the associated defect $[V_F^-–V_o–V_F^-]$ into an even more stable neutral one $[V_c–V_o]$, which is optically inactive, i.e., $V_o + [V_F^-–V_o–V_F^-] \rightarrow 2[V_c–V_o] + 2\,h$. When the annealing temperature becomes much higher (1040 °C), a Schotty defect reaction will occur due to the evaporation of PbO, i.e., $PWO \rightarrow V_c + V_o + PbO\ (gas)$. A stable dipole $[V_c–V_o]$ will be formed, and the interstitial oxygen can gain enough energy to diffuse to the surface and to overcome the surface-absorption energy to diffuse into the air.[10,27,28] So, the absorption intensity at 350 nm of the 1040 °C annealed sample will decrease.

3.3. Judd–Ofelt analysis

The room-temperature absorption spectrum is analysed in the framework of the Judd-Ofelt theory[30,31] to determine the radiative transition rates and the luminescence branching ratio for the $^4F_{3/2}$ metastable level. An expression for theoretical oscillator strength f^{cal} is constructed using the reduced matrix elements from Ref. [32]. The experimental oscillator strength f^{exp} evaluated by a numerical integration of the absorption bands shown in Fig. 2 is used as the input data for the calculation. Results of the fitting are given in Table 2.

Table 2. Measured and calculated oscillator strengths for Nd^{3+} in $PbWO_4$.

Transition (from $^4I_{9/2}$)	λ_{abs}/nm	FWHM/nm	$f^{exp}/10^{-6}$	$f_{md}/10^{-6}$	$f_{ed}^{exp}/10^{-6}$	$f_{ed}^{cal}/10^{-6}$
$^4F_{3/2}$	876	24	1.5410	–	1.5410	1.7920
$^4F_{5/2}+^2H(2)_{9/2}$	804	15	4.2219	0.02464	4.1973	4.4406
$^4F_{7/2}+^4S_{3/2}$	752	16	3.8592	–	3.8592	3.7750
$^4F_{9/2}$	685	15	0.3299	0.0044	0.3255	0.3328
$^2H_{11/2}$	629	10	0.0884	–	0.0884	0.0916
$^4G_{5/2}+^2G(1)_{7/2}$	586	17	27.8165	0.00044	27.8161	27.8712
$^2K_{13/2}+^4G_{7/2}+^4G_{9/2}$	525	8	5.9752	–	5.9752	5.0275
$^2K_{15/2}+^2G(1)_{9/2}+^2D(1)_{3/2}+^4G_{11/2}$	478	11	1.1332	–	1.1332	0.8685
$^2P_{1/2}$	431	4	0.3894	–	0.3894	0.5039

The experimental oscillator strength f^{exp} can be obtained by using the following equation:

$$f^{exp} = \frac{mc^2}{\pi e^2 \lambda^2 N} \int \alpha(\lambda)\,\mathrm{d}\lambda, \tag{1}$$

where m and e are the mass and the charge of the electron, c is the speed of light, α is the absorpton coefficient at wavelength λ, and $N = 0.5165\times10^{20}\ \mathrm{cm}^{-3}$. It is composed of the oscillator strengths of the electronic-dipole transition (f_{ed}) and the magnetic-dipole transition (f_{md}), i.e.,

$$f = f_{ed} + f_{md}, \tag{2}$$

$$f_{md} = \chi_{md} f', \quad \chi_{md} = n, \tag{3}$$

$$f_{ed}^{exp} = \frac{8\pi^2 mc\sigma}{3h(2J+1)} \chi_{ed} \sum_{t=2,4,6} \Omega_t U(t),$$

$$\chi_{\rm ed} = \frac{(n^2+2)^2}{9n}, \tag{4}$$

where f' is a constant related to the electronic-dipole transition from the ground state to the excited state and can be obtained in Ref. [32], n is the refraction index, h is the Planck constant, σ is the wavelength number of the corresponding transition, J is the quantum number of the total angular momentum, Ω_t is the Judd–Ofelt parameter of the transition, and U is the matrix element of the transition from the ground state to the excited state. The theoretical oscillator strength of the electronic-dipole transition ($f_{\rm ed}^{\rm cal}$) can be obtained with the expression

$$f_{\rm ed}^{\rm cal} = \frac{8\pi^2 mc}{3h\lambda(2J+1)}\chi_{\rm ed}\sum_{t=2,4,6}\Omega_t U(t), \tag{5}$$

where $\chi_{\rm ed} = (n^2+2)/9n$.

The Judd–Ofelt parameters ($\Omega_{2,4,6}$) can be obtained by fitting the experimental oscillator strength to the calculated one using the least square technique. With parameters $\Omega_{2,4,6}$ determined ($\Omega_2 = 5.04\times10^{-20}$ cm^2, $\Omega_4 = 2.31\times10^{-20}$ cm^2, $\Omega_6 = 1.52\times10^{-20}$ cm^2, RMS $= 0.1407\times10^{-6}$), the radiative transition rate $W_{\rm r}$ and the luminescence branching ratio β for the $^4F_{3/2}$ level can be calculated and gathered in Table 3. The equations used are listed below. The $^4F_{3/2}$ radiative lifetime $\tau_{\rm r}$ defined as the inverse of the sum of radiative transition rates is found to be 271 μs.

$$W_{\rm r} = W_{\rm r,ed} + W_{\rm r,md}, \tag{6}$$

$$W_{\rm r,ed} = \frac{64\pi^4 e^2}{3h\lambda^3(2J+1)}\chi'_{\rm ed}\sum_{t=2,4,6}\Omega_t U(t), \tag{7}$$

$$W_{\rm r,md} = \frac{4\pi^2 e^2 h}{3m^2c^2\lambda^3(2J+1)}\chi'_{\rm md} \times \langle SLJ\,\|L+2S\|\,S'L'J'\rangle^2, \tag{8}$$

where $\chi'_{\rm ed} = n(n^2+2)^2/9$, $\chi'_{\rm md} = n^3$, S, L, and J are the quantum numbers of the total spin angular momentum, the total angular momentum, and the orbital angular momentum, respectively.

Table 3. Calculated values of radiative transition rate $W_{\rm r}$ and branching ratio β for $^4F_{3/2}$ level of Nd^{3+} in $PbWO_4$.

Transition (from $^4F_{3/2}$)	Transition wavelength/nm	$W_{\rm r}$/s^{-1}	β/%
$^4I_{9/2}$	876	1878.31	50.9
$^4I_{11/2}$	1061	1525.71	41.3
$^4I_{13/2}$	1332	275.50	7.5
$^4I_{15/2}$	1851	14.18	0.38

3.4. Room-temperature luminescence spectra of Nd^{3+} ions in $PbWO_4$

Figure 3 shows the luminescence spectra around 1.06 μm of the as-grown and the 1040 °C annealed Nd-doped $PbWO_4$ crystals. We can see that the luminescence intensity at 1061 nm increases gradually with the increase of the concentration of Nd^{3+} ions. The peak emission cross-section at 1061 nm is calculated by using the Fuchtbauer–Ladenburg equation, i.e.,

$$\sigma_{\rm em}(\lambda) = \frac{\beta\lambda^5}{8\pi cn^2\tau_{\rm rad}} \times \frac{I(\lambda)}{\int I(\lambda)\,\lambda {\rm d}\lambda},$$

where $\tau_{\rm rad}$ is the radiative lifetime. For $^4F_{3/2} \rightarrow {}^4I_{11/2}$ transition, $\beta = 0.41$, $\tau_{\rm rad}$ is the radiative lifetime of the $^4F_{3/2}$ level given in the above section. The emission cross-sections are 4.84×10^{-20} cm^2, 5.82×10^{-20} cm^2, and 5.90×10^{-20} cm^2 for as-grown samples A, B, and C, respectively. It can be found that the luminescence intensity increases after the 1040 °C annealing treatment. They are 6.03×10^{-20} cm^2, 6.36×10^{-20} cm^2, and 5.17×10^{-20} cm^2 for annealed samples A, B, and C, respectively. The annealing treatment in air can effectively modulate the microstructure of the as-grown $PbWO_4$ crystal through reducing the intrinsic defects, which improves its radiation intensity and optical performances. The emission cross-section of Nd^{3+}-doped $PbWO_4$ crystal is much smaller than those of Nd^{3+}-doped vanadate and tungstate crystals, such as Nd^{3+}-YVO_4 (135×10^{-20} cm^2), Nd^{3+}-$GdVO_4$ (76×10^{-20} cm^2), Nd^{3+}-$LuVO_4$ (146×10^{-20} cm^2), Nd^{3+}-KYW (44×10^{-20} cm^2), Nd^{3+}-KGW (39×10^{-20} cm^2), and Nd^{3+}-KLuW (21×10^{-20} cm^2).[20–26]

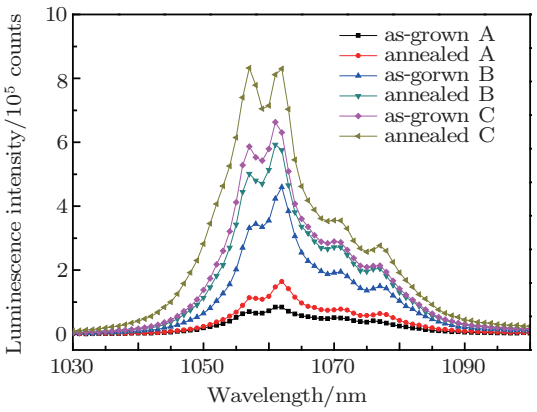


Fig. 3. (colour online) Emission spectra at 1.06 μm region of the as-grown and the 1040 ° annealed samples.

Figure 4 shows the semilog plots of the Nd^{3+} luminescence decay curves of Nd-doped $PbWO_4$ crystals. For the as-grown crystals, the lifetime of the $^4F_{3/2}$ level decreases from 192 μs to 164 μs with the doping concentration increasing from 0.2 at.% to 1.0 at.%. It is because [Nd^{3+}–Nd^{3+}] clusters will be formed as the doping concentration increases. The cross relaxation induced by the interaction between Nd^{3+} ions in [Nd^{3+}–Nd^{3+}] clusters will improve the nonradiative transition of the $^4F_{3/2}$ level. Annealing at high temperature can improve the crystal quality and eliminate the structural defects. So the energy transfer from the Nd^{3+} ions to the structural defects will decrease, which induces the increase of the fluorescence lifetime of Nd^{3+}. Compared with Nd^{3+}-doped vanadate (Nd^{3+}-YVO_4: 76 μs, Nd^{3+}-$GdVO_4$: 90 μs, Nd^{3+}-$LuVO_4$: 82 μs) and tungstate (Nd^{3+}-KYW: 99 μs, Nd^{3+}-KGW: 104 μs, Nd^{3+}-KLuW: 110 μs) crystals, Nd^{3+}-doped $PbWO_4$ crystal has a longer fluorescence lifetime at the wavelength of 1060 nm.[20–26]

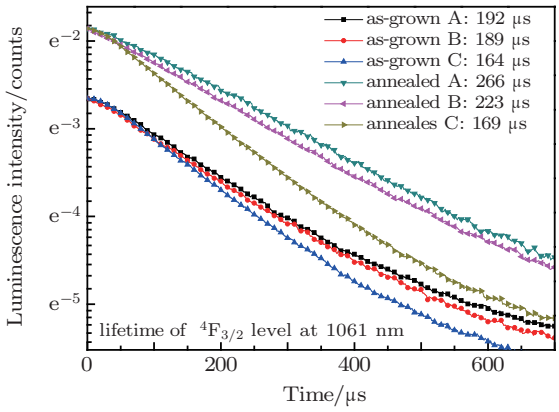


Fig. 4. (colour online) Nd^{3+} luminescence decay curves of the as-grown and the 1040 ° annealed Nd-doped $PbWO_4$ crystals.

3.5. Raman spectra

The spontaneous backscattering Raman spectra of the three crystals are recorded at the $a(cc)\bar{a}$ excitation geometry and shown in Fig. 5. There are 5 Raman peaks found in the spectra, i.e., 903 cm^{-1}, 766 cm^{-1}, 357 cm^{-1}, 326 cm^{-1}, and 178 cm^{-1}. According to Refs. [33]–[36], the 903 cm^{-1} peak corresponds to the [W–O] symmetric stretching vibrational mode (A_g), the 766 cm^{-1} peak corresponds to the [W–O] antisymmetric stretching vibrational mode (B_g), the 357 cm^{-1} peak corresponds to the [O–W–O] antisymmetric bending vibrational mode (B_g), the 326 cm^{-1} peak corresponds to the [O–W–O] symmetric bending vibrational mode (A_g), and the 178 cm^{-1} peak corresponds to the [WO_4^{2-}] rotation vibrational mode. We also find a broadband peak at around 2660 cm^{-1}, which maybe originates from the interaction between the input photons and the Nd^{3+} ions. The excitation source used in the measurement is a 514 nm laser, and it is overlapped with the absorption band of the transition $^4I_{9/2} \rightarrow {}^2K_{13/2} + {}^4G_{7/2} + {}^4G_{9/2}$. Under 514 nm laser pumping, we observe visible fluorescence peaks at 515 nm ($^4G_{9/2} \rightarrow {}^4I_{9/2}$), 613 nm ($^4G_{5/2} \rightarrow {}^4I_{9/2}$), and 670 nm ($^4F_{9/2} \rightarrow {}^4I_{9/2}$).

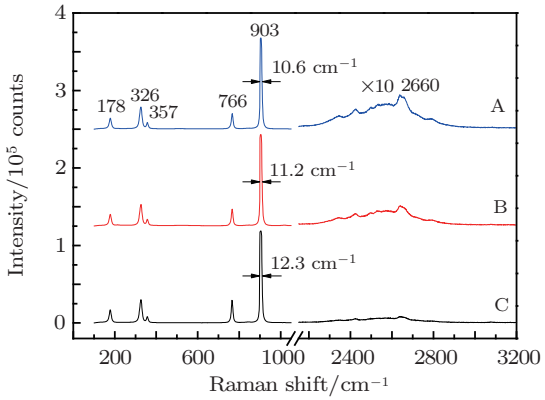


Fig. 5. (colour online) Spontaneous backscattering Raman spectra of the crystals obtained with $a(cc)\bar{a}$ excitation geometry.

The most intense vibrational mode of Nd-doped $PbWO_4$ crystal is at 903 cm^{-1}, with the Raman line widths being 12.3 cm^{-1}, 11.1 cm^{-1}, and 10.6 cm^{-1}, respectively. The vibronic Raman mode dephasing time T_R can be obtained using equation $\Delta\Omega_R = (\pi c T_R)^{-1}$. The steady-state SRS gain can be characterized by the peak intensity, and the transient state SRS gain can be characterized by the integral cross section. Raman frequency Ω_R, Raman line width $\Delta\Omega_R$, peak intensity Σ_{peak}, vibronic Raman mode dephasing time T_R, and integral cross section Σ_{int} of Nd-doped $PbWO_4$ crystals are shown in Table 4.[35,37] A large peak and integral Raman scattering cross-sections are observed in the $PbWO_4$ crystal. The Raman spectroscopic properties of vanadate and tungstate crystals have been widely investigated. The Raman frequency Ω_R, Raman line width $\Delta\Omega_R$, and vibronic Raman mode dephasing time T_R of these crystals are reported as follows: YVO_4: 890 cm^{-1}, 3 cm^{-1}, and 3.5 ps; $GdVO_4$: 882 cm^{-1}, 12.8 cm^{-1}, and 0.8 ps; KYW: 905.6 cm^{-1}, 7 cm^{-1}, and 1.9 ps; and KGW: 901 cm^{-1}, 5.4 cm^{-1}, and 1.4 ps.[38–42] It can be found that the Raman properties of $PbWO_4$ crystal are comparable to those of the popular Raman crystals.

Table 4. Spontaneous Raman scattering properties of Nd-doped $PbWO_4$ crystals.

Crystal	Molecular group	Ω_R/cm^{-1}	$\Delta\Omega_R/cm^{-1}$	$\Sigma_{peak}/10^5$ arb. units	T_R/ps	$\Sigma_{int}/10^6$ arb. units	Geometry
A	$[WO_4]$	903	12.3	1.18	0.86	1.64	$//c$
B	$[WO_4]$	903	11.2	1.17	0.96	1.51	$//c$
C	$[WO_4]$	903	10.6	1.17	1.0	1.45	$//c$

4. Conclusion

Nd-doped $PbWO_4$ crystals with different concentrations are grown by using the modified Bridgman method. The absorption cross-sections of the three crystals at 808 nm are found to be 2.85×10^{-20} cm^2, 3.11×10^{-20} cm^2, and 2.88×10^{-20} cm^2, respectively. Under 808 nm LD pumping, the peak emission cross-sections at 1060 nm are 4.84×10^{-20} cm^2, 5.82×10^{-20} cm^2, and 5.90×10^{-20} cm^2, respectively. The changes of the absorption band at 350 nm are discussed for the samples annealed at 740 °C and 1040 °C. The radiative lifetime of the $^4F_{3/2}$ level is calculated using the Judd–Ofelt theory according to the absorption spectrum of 0.5 at.% Nd-doped $PbWO_4$ crystal. The spontaneous Raman scattering properties of the crystals are investigated.

Acknowledgement

We are grateful to Dr. Piotr Solarz (Institute of Low Temperature and Structure Research, Polish Academy of Sciences (ILTSR)) for comments on preparing the manuscript.

References

[1] Huang Y H, Jiang D L, Zhang J X and Lin Q L 2010 *Acta Phys. Sin.* **59** 300 (in Chinese)
[2] Huang T D, Jiang B X, Wu Y S, Li J, Shi Y, Liu W B, Pan Y B, Huang L P and Guo J K 2009 *Acta Phys. Sin.* **58** 1298 (in Chinese)
[3] Xie W, Wang Y H, Hu Y H, Wu H Y, Deng L Y and Liao F 2010 *Acta Phys. Sin.* **59** 1148 (in Chinese)
[4] Xie W, Wang Y H, Hu Y H, Luo L, Wu H Y and Deng L Y 2010 *Acta Phys. Sin.* **59** 3344 (in Chinese)
[5] Zhang Y 2010 *Acta Phys. Sin.* **59** 5528 (in Chinese)
[6] Yang Z P, Ma X, Zhao P P and Song Z P 2010 *Acta Phys. Sin.* **59** 5387 (in Chinese)
[7] Wang D G, Zhou Y X, Wang X S, Dai S X, Shen X, Chen F F and Wang S 2010 *Acta Phys. Sin.* **59** 6256 (in Chinese)
[8] Grabtchikov A S, Kuzmin A N, Lisinetskii V A, Orlovich V A, Ryabtsev G I and Demidovich A A 1999 *Appl. Phys. Lett.* **75** 3742
[9] Kroger F A 1948 *Some Aspects of the Luminescence of Solids* (Amsterdam: Elsevier)
[10] Chen Y J, Lin Y F, Luo Z D and Huang Y D 2005 *J. Opt. Soc. Am.* B **22** 898
[11] Kaminskii A A, McCray C L, Lee H R, Lee S W, Temple D A, Chyba T H, Marsh W D, Barnes J C, Annanenkov A N, Legun V D, Eichler H J, Gad G M A and Ueda K 2000 *Opt. Commun.* **183** 277
[12] Moreau J M, Galez P, Peigneux J P and Korzhik M V 1996 *J. Alloys Compd.* **238** 46
[13] Nikl M, Nitsch K, Baccaro S, Cecilia A, Montecchi M, Borgia B, Dafinei I, Martini M, Rosetta E, Spinolo G, Vedda A, Kobayashi M, Ishii M, Usuki Y, Jarolimek O and Reiche O 1997 *J. Appl. Phys.* **82** 5758
[14] Annenkov A, Auffray E, Korzhik M, Lecoq P and Peigneux J P 1998 *Phys. Stat. Sol.* A **170** 47
[15] Kaminskii A A, Eichler H J, Ueda K, Klassen N V, Redkin B S, Li L E, Findeisen J, Jaque D, Garcia-Sole J, Fernandez J and Balda R 1999 *Appl. Opt.* **38** 4533
[16] Chen W B, Inagawa Y, Omatsu T, Tateda M, Takeuchi N and Usuki Y 2001 *Opt. Commun.* **194** 401
[17] Gad G M A, Eichler H J and Kaminskii A A 2003 *Opt. Lett.* **28** 426
[18] Mirov I S, Fedorov V V, Moskalev I S, Martyshkin D V, Beloglovski S Y, Burachas S F, Saveliev Y A and Tseitline A M 2008 *Opt. Mater.* **31** 94
[19] Yang P Z, Liao G J, Shen B F, Shao P F, Ni H H and Yin Z W 2002 *J. Cryst. Growth* **236** 589
[20] Lomheim T S and Deshazer L G 1978 *J. Appl. Phys.* **49** 5517
[21] Lavi R, Jackel S, Tal A, Lebiush E, Tzuk Y and Goldring S 2001 *Opt. Commun.* **195** 427
[22] Xie G Q, Tang D Y, Luo H, Yu H H, Zhang H J and Qian L J 2008 *Laser Phys. Lett.* **5** 647
[23] Kaminskii A A, Bettinelli M, Dong J, Jaque D and Ueda K 2009 *Laser Phys. Lett.* **6** 374
[24] Schawlow A L and Townes C H 1958 *Phys. Rev.* **112** 1940
[25] Kaminskii A A, Verdun H R, Koechner W, Kuznetsov F A and Pavlyuk A A 1992 *Kvantovaya Elektronika* **19** 941
[26] Guo L H, Yang W Q and Feng S Y 2007 *J. Synthetic Cryst.* **36** 475
[27] Zhu W L, Feng X Q, Wu Z H and Man Z Y 2002 *Physica* B **324** 53
[28] Huang Y L, Feng X Q, Xu Z H, Zhao G J, Huang G S and Li S G 2003 *Solid State Commun.* **127** 1
[29] Lin Q S, Feng X Q, Man Z Y, Shi Z S and Zhang Q R 2000 *Phys. Stat. Sol.* A **181** R1
[30] Judd B R 1962 *Phys. Rev.* **127** 750
[31] Ofelt G S 1962 *J. Chem. Phys.* **37** 511
[32] Carnall W T, FieldsP R and Rajnak K 1968 *J. Chem. Phys.* **49** 4424
[33] Zhu W L, Wan K S, Huang Y L, Feng X Q and Pezzotti G 2006 *Phys. Stat. Sol.* A **203** 2376

[34] Kaminskii A A, Bagayev S N, Ueda K, Nishioka H, Kubotay Y, Chen X and Kholov A 1995 *Jpn. J. Appl. Phys.* **34** L1461

[35] Basiev T T, Sobol A A, Zverev P G, Ivleva L I, Osiko V V and Powell R C 1999 *Opt. Mater.* **11** 307

[36] Xiong W, Chen L and Yuan H 2010 *J. Synth. Cryst.* **39** 5

[37] Basiev T T, Sobol A A, Zverev P G, Osiko V V and Powell R C 1999 *Appl. Opt.* **38** 594

[38] Basiev T T, Sobol A A, Zverev P G, Ivleva L I, Osiko V V and Powell R C 1999 *Opt. Mater.* **11** 307

[39] Kaminskii A A, Eichler H J, Ueda K, Klassen N V, Redkin B S, Li L E, Findeisen J, Jaque D, Garcia-Sole J, Fernandez J and Balda R 1999 *Appl. Opt.* **38** 4533

[40] Kaminskii A A, McCray C L, Lee H R, Lee S W, Temple D A, Chyba T H, Marsh W D, Barnes J C, Annanenkov A N, Legun V D, Eichler H J, Gad G M A and Ueda K 2000 *Opt. Commun.* **183** 277

[41] Kaminskii A A, Ueda K, Eichler H J, Kuwano Y, Kouta H, Bagaev S N, Chyba T H, Barnes J C, Gad G M A, Murai T and Li J R 2001 *Opt. Commun.* **194** 201

[42] Hu D W, Wang Z P, Zhang H J, Xu X G, Wang J Y and Shao Z S 2008 *Chinese J. Lasers* **35** 11